 doi:10.20944/preprints202101.0270.v1

Article

Scaling of measure fluctuations on a flapping flag device in the open channel around a cylinder at $Re = 10^4$: Taylor's law approach

Samuele De Bartolo [1], Massimo De Vittorio [1,3], Antonio Francone [1], Francesco Guido [3], Elisa Leone [1], Vincenzo Mastronardi [3], Andrea Notaro [1,2*] and Giuseppe Roberto Tomasicchio [1]

1 University of Salento, Department of Engineering for Innovation, EUropean Maritime Environmental Research (EUMER), Via per Monteroni, 73100 Lecce, Italy ;
2 School of Advanced Studies ISUFI, University of Salento, Via per Monteroni, 73100 Lecce, Italy;
3 Italian Institute of Technology (IIT), Center for Biomolecular Nanotechnologies (CBN), Via Barsanti 14, 73100 Arnesano (Lecce), Italy;
4 Polytechnic of Bari, Department of Civil, Environmental, Land, Construction and Chemistry Engineering, Via Edoardo Orabona 4, 70125 Bari, Italy
* Correspondence: andrea.notaro@studenti.unisalento.it

Abstract: Experimental evidence showed how various complex systems, characterized by a fluctuation scaling, satisfy the well-known Taylor's law. The present work aims to apply for the first time Taylor's law, given its general treatment, for a flow field at Re around 10^4, since activity of each fluid particle is highly fluctuating, especially in the context of vortex shedding. In addition, the further element of innovation is the use of an innovative thin-films based device consisting of an elastic piezoelectric flapping flag that is proposed as a measuring instrument of the flow field. The oscillations of the flapping flag, due to the vortexes release downstream to an obstacle of cylindrical shape, generate an alternating piezoelectric voltage whose time history is similar to the chaotic components of the fully developed turbulent speed. Preliminary experimental results about the use of thin-films based device in a flume channel are reported together with a second order analysis on the voltage difference and a scaling law of the exponent scale.

Keywords: sensors technologies, sensor systems for water flow, hydrodynamics monitoring of rivers, hydraulics, MEMS, Fluid-structure interactions

1. Introduction

In the previous years, the development of fluid-dynamic measuring instruments is steadily increasing. Especially the influence due to the presence of a body in a uniform flow with the consequent vortexes release is even today an object of interest. As it is well known, vortex shedding phenomenon is governed by Strouhal number that represents the ratio of inertial forces due to the local acceleration of the flow to the inertial forces due to the convective acceleration [16]. Several studies aimed to define the relationship between Strouhal and Reynolds number have followed each other through the years. Originally [33], measurements on a large circular cylinder in a pressurized wind tunnel at Reynolds numbers from 10^6 to 10^7 have revealed a high Reynolds number transition in which the drag coefficient increases from its low supercritical value to a value 0.7 at $Re = 3.5 \cdot 10^6$ and then becomes constant. Also, for $Re > 3.5 \cdot 10^6$, a definite vortex shedding occurs, with Strouhal number 0.27. According to the experiment of Bearman [3], vortex shedding frequencies were measured by using a model with splitter plates, in which an oscilloscope displaying the fluctuating voltage of a hot wire gave an accurate picture of the velocity fluctuation at the hot-wire probe. In the same way, a constant value of $St = 0.178$ was found by Griffin [13] for subcritical wake Reynolds numbers from 700 to $5 \cdot 10^4$. Okajima [27] determined Strohual numbers of rectangular cylinders as a function of Reynolds

Preprints (www.preprints.org) | NOT PEER-REVIEWED | Posted: 14 January 2021 doi:10.20944/preprints202101.0270.v1

number in the range between 70 and $2 \cdot 10^4$, using an open-jet small wind tunnel and a towing-type water tank. A sudden discontinuity in the Strouhal-number curves was noted for a ratio width/height of the cylinder in the range between 2 and 3, highlighting the strong dependence on dimensional characteristics. Few years later, Gonçalves and Vieira [12] performed a set of experiments in a pilot vertical low turbulence hydrodynamic tunnel, where the emission of liquid dye directly in non-perturbed flow by means of a long hypodermic needle has been utilized to create the flow image captured by a A3 CCD high-resolution video camera in order to determinate Strouhal number for Reynolds up to 600, as a result of processing. Taylor et al. [38] have shown that birds, bats and insects in a cruising flight flap their wings within a narrow range of Strohual number $0.2 < St < 0.4$, since the animals tune their frequency to achieve maximum propulsive efficiency. More recently, Eloy [9] predicted the optimal Strohual number for swimming animals by the use of Lighthill's large-amplitude elongated-body theory. With the spread of optical methods, the Particle Image Velocimetry (PIV) technique has been used by Shi et al. [35] to visualize the vortex shedding processes from parallel-plate thermoacoustic stacks in oscillatory flow conditions within an acoustic cycle, phase-by-phase, in particular during the part of the cycle when the fluid flows out of the stack – selected cases are shown for comparisons with hot wire measurements. The wake characteristics and the vortex shedding process in the flow past a circular cylinder may also be studied through Large eddy simulation (LES), which is a mathematical model for turbulence used in computational fluid dynamics, as made by Rodriguez et al. [31] for the range of Reynolds numbers $2.5 \cdot 10^5 < Re < 8.5 \cdot 10^5$. The use of the thin films-based device is proposed as an alternative for the instruments used in the experiments previously mentioned; a general view of that will be seen in the section 2. In the present work a fluctuating signal of 30 minute has been taken as a reference, in order to avoid the danger related to the resonance phenomenon. In fact, if the frequency of vortex shedding matches the resonance frequency of the structure, it begins to resonate and vibrates in harmonic oscillations driven by the energy of the flow. Subsequently, vibrations rise and structure can be damaged or deformed permanently. For the long-term vibration, fatigue stress and subsequently fatigue failure is significant [14]. As described in Section 3, once acquired the signal of the voltage fluctuations recorded by the thin films-based device, a second order theory based on mean and variance has been applied to experimental voltages data in order to recognize a scaling power law, evaluate the development of scale exponent over time, and characterize some aspects of turbulence, such as statistical distribution and the ergodicity. Finally, in Section 4, a critical discussion of results is undertaken.

2. Materials and Methods

The thin-films based device, previously mentioned, consists of a flag, clamped at a cylinder [20,23], which oscillates in a media flow, as shown in figure 1a, and converts kinetic energy into electrical energy [29].

The variables involved in this problem are the following: frequency of vortex shedding f_r, height of the open channel h, diameter of cylinder D, length of flag l, bulk velocity U, kinematic viscosity ν. Since the reference dimensions are two (length and time), according to Buckingham Theorem we have four independent dimensionless groups, among them Strouhal and Reynolds numbers. Therefore, we need to establish the values of Reynolds and Strouhal numbers for the flow field in which this experiment occurs. The experimental set-up is reported in figure 1b showing the channel flume, site in EUMER Lab at University of Salento, where is located the flag, whose Modulus of Young is equal to E = 2.5 GPa, clamped at the end to a cylinder of diameter D = 2.00 cm. The density and kinematic viscosity of the water are equals to $\rho = 1000\ kg\ m^{-3}$ and $\nu = 10^{-6}\ m^2\ s^{-1}$ at the temperature of 25 C respectively. The flag device acts as a flexible piezoelectric transducer. It is mainly based on a polyimide substrate (Kapton 100HN, 25 μm of thickness), on which a multilayered structure was grown and microfabricated in order to guarantee high sensitivity and flexibility. A detailed sketch is reported in figure 2.

Preprints (www.preprints.org) | NOT PEER-REVIEWED | Posted: 14 January 2021 doi:10.20944/preprints202101.0270.v1

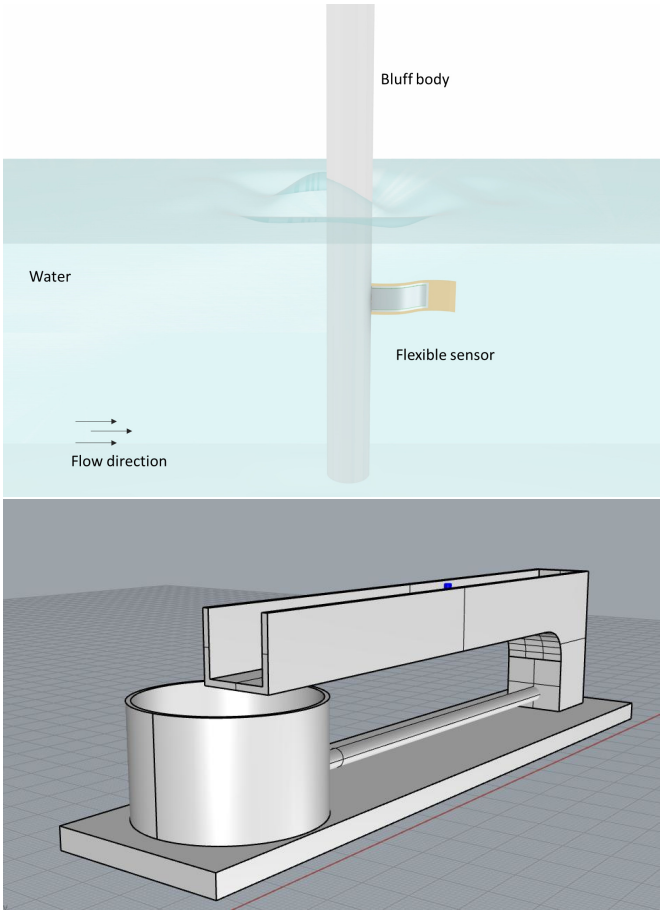

Figure 1. The sensor, mounted downstream of the bluff body, is affected by the vortexes and oscillates generating alternating voltage (a). 3d view of the channel flume site in EUMER Lab of Unversity of Salento (b)

Preprints (www.preprints.org) | NOT PEER-REVIEWED | Posted: 14 January 2021 doi:10.20944/preprints202101.0270.v1

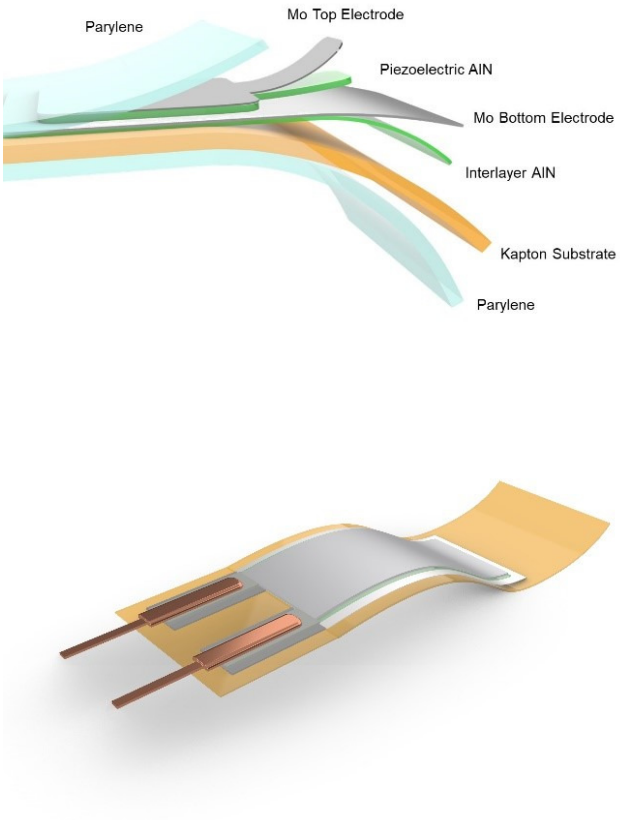

Figure 2. The flexible structure of the piezoelectric devices was optimized to guarantee high flexibility and sensitivity. In addition all the materials used for its fabrication are completely biocompatible, suitable for environmental use (a). The 3D sketch highlights the extremely compactness of the transducer (b).

Preprints (www.preprints.org) | NOT PEER-REVIEWED | Posted: 14 January 2021 doi:10.20944/preprints202101.0270.v1

The multi-layered thin films structure consists of a piezoelectric layer of Aluminum Nitride (AlN, 1 μm thick) sandwiched between two Molybdenum films (Mo, 200 nm of thickness) acting as electrodes. AlN is a dielectric material presenting interesting electrical and a natural piezoelectricity due to its crystal symmetry [1,19,26,28]. Since the device will be employed as an underwater sensor, it needs to be fully electrically insulated. For this reason, a thin film of Parylene-C (1.5-2.5 μm) is uniformly deposited, at room temperature. This insulating layer covers the final device in a conformal way, making it perfectly waterproof. The dimensions of the active piezoelectric area are 1.7 x 0.4 cm^2 and it is positioned at the hinge of the flapping structure, where the mechanical stress is higher during the flapping-induced oscillations. To fabricate the flexible devices, standard microfabrication procedures as photolithography, wet and dry etching processes were performed. In addition, a CNC laser cutter was used to define the elastic substrate geometry. The last step of the fabrication process consisted from the mechanical crimping of the electrodes in order to connect the device, allowing the reading and post processing of the electrical voltage signal generated by the piezoelectric film. The part of the device with the electrical connections was then embedded into the cylindrical bluff body, keeping still the connections waterproof. The voltage fluctuations $\mathbf{v}(t)$ generated by mode shapes and deflections of the flapping flag, shown in figure 3a, due to the flow field were then recorded by an oscilloscope (Tektronix, MSO2000B) (see figure 3b).

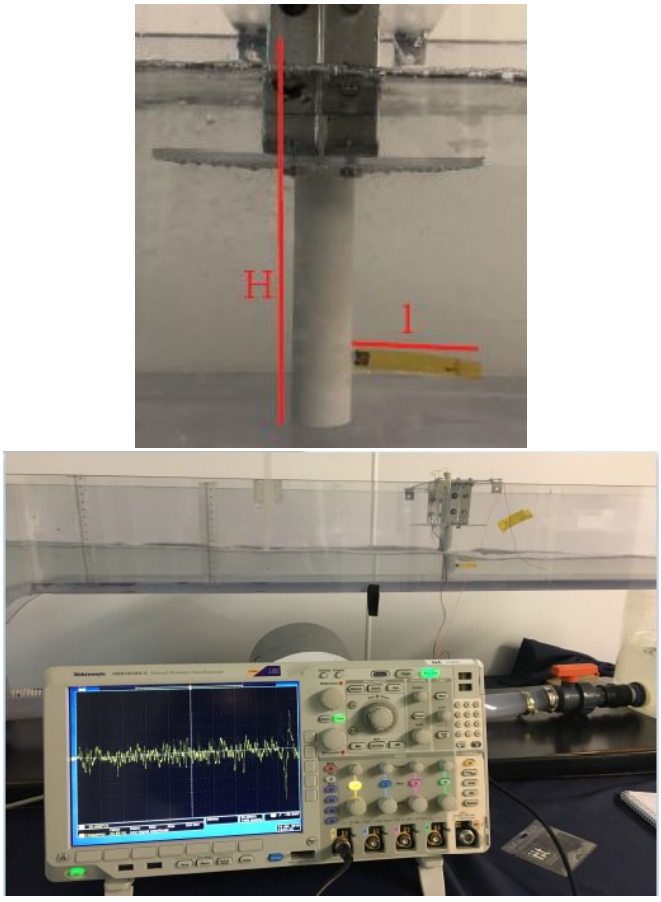

Figure 3. Flapping flag clamped at the cylinder (a) and Oscilloscope Tektronix MSO2000B (b)

Once a steady inlet flow rate was set, four different configurations have been studied. In the first two configurations flag length is l = 3.20 cm, with bulk velocity U equal to 0.297 $m\ s^{-1}$ (figure 5a) and 0.342 $m\ s^{-1}$ (figure 5b) for Reynolds numbers Re = 5944 and Re = 6835 respectively. Instead, in the last two configurations the flag length is l = 7.90 cm (figures 5c and 5d), with the same values of bulk velocity U (0.297 $m\ s^{-1}$ and 0.342 $m\ s^{-1}$) and Reynolds number Re (5944 and 6835). According to continuity equation, in stationary

Preprints (www.preprints.org) | NOT PEER-REVIEWED | Posted: 14 January 2021 doi:10.20944/preprints202101.0270.v1

case, bulk velocity is given by $U = Q/(Bh)$ in which $B = 0.16\ m$ is the width of the channel flume, whereas h is the height of the flow in the open channel set by means some hydraulic systems reducing the flow section upstream of the cylinder (figures 4 and 5).

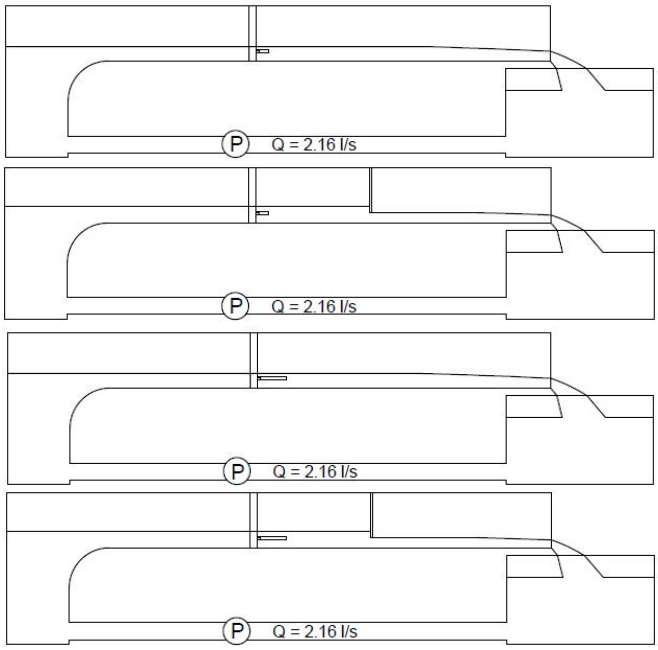

Figure 4. Longitudinal section of the channel flume at EUMER Lab of University of Salento for the following configurations: first (a), second (b), third (c) and fourth (d).

As we know, the presence of the cylinder immersed in this uniform stream is a source of turbulence, therefore large eddies are shed downstream. These vortexes are formed at a regular frequency that we can determinate through Strouhal number St defines as [36]:

$$St = \frac{f_r\ D}{U} \tag{1}$$

where f_r is the frequency of vortex shedding from one side of the cylinder (in s^{-1}), U is the bulk velocity and D is the diameter of cylinder. Since in Section 1, we have stated that four dimensionless groups are included in this problem and hence Strohual number may be express as a function of the other: $St = f(H/D, l/D, 1/Re)$, it is important to understand the relationship with Reynolds number. If we consider the equation 1 the value of frequency obtained applying Fast Fourier Transform (FFT) to the fluctuating signal and plot experimental data (the four crosses in black, **x**) in a plane in which are collected points corresponding to different diameters of the cylinder [32], we are in the plateau zone as expected for our flow regime (figure 6).

Then, our efforts have been focused on identifying a scaling power law based on experimental data. *Taylor's law*, also known as fluctuation scaling in physics [8], is one of the most verified patterns in both the biological and physical sciences [10]. It states that with respect to a non-negative stochastic variable X, the variance V=Var[X], or equivalently σ^2, is a power function of its mean $\mu = E[X]$:

$$V = a\mu^b \tag{2}$$

where a and b are both positive constants [18], in particular b is called scaling exponent. It is titled by Taylor [37] who was the first that proposed it after he surveyed some classical population such as virus lesions, macro zoo-plankton, worms and symphylids in the soil, on the plants and in the air, mites on leaves, ticks on sheep and fish in the sea. Given its

Preprints (www.preprints.org) | NOT PEER-REVIEWED | Posted: 14 January 2021 doi:10.20944/preprints202101.0270.v1

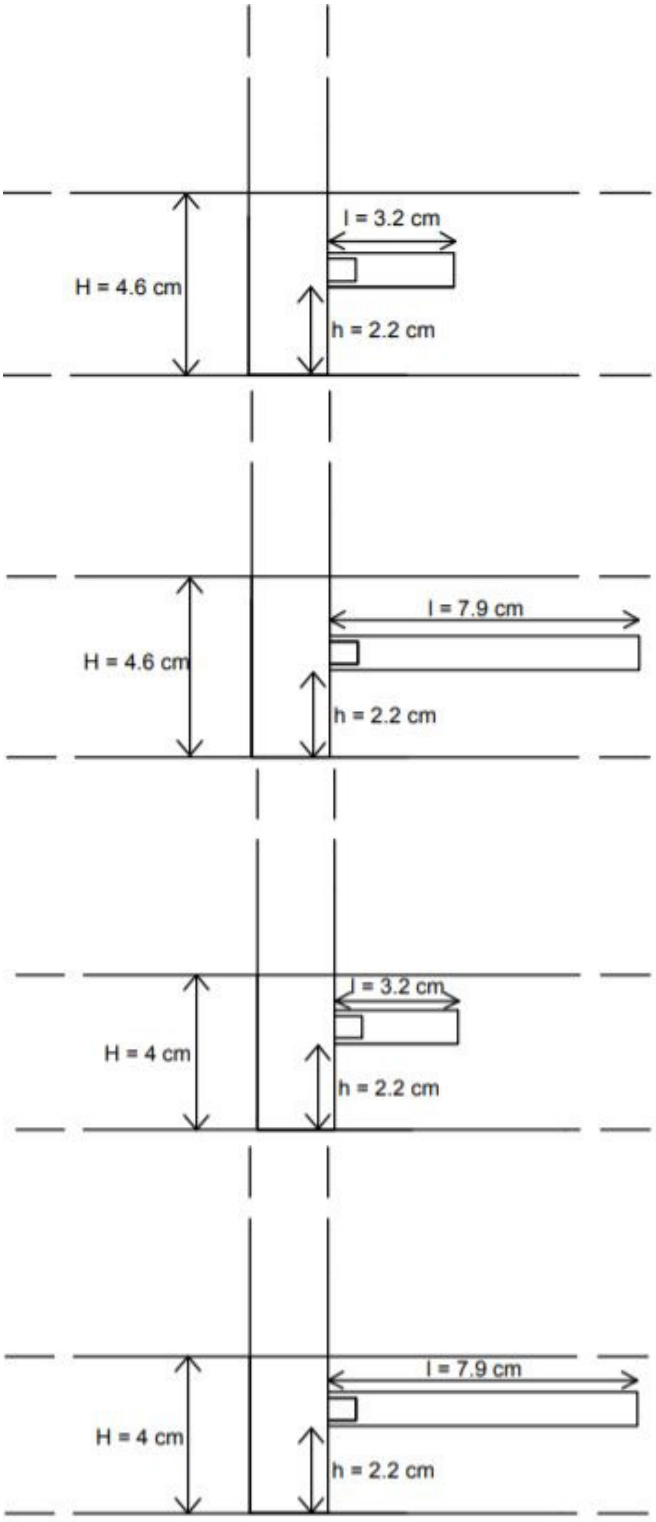

Figure 5. Details of the flag clamped at the cylinder for the following configurations: first (a), second (b), third (c) and fourth (d).

Preprints (www.preprints.org) | NOT PEER-REVIEWED | Posted: 14 January 2021 doi:10.20944/preprints202101.0270.v1

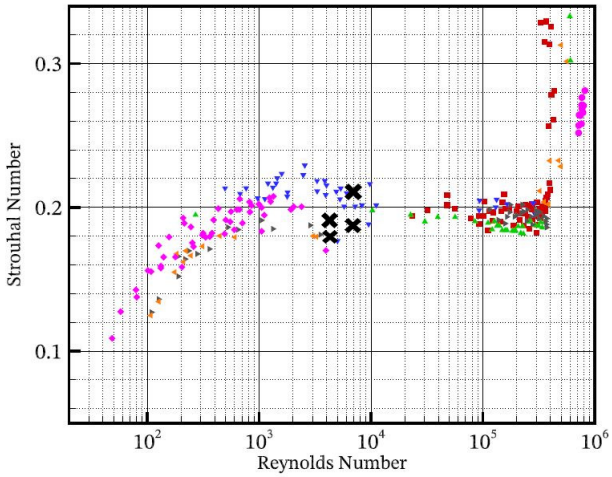

Figure 6. Strouhal number - Reynolds number relationship for circular cylinders, from [32]

generality, Taylor's law can be applied to many fields of study. In ecology, the random variable of interest is generally the size or density N of a censused population and Taylor's Law can arise in time or in space [11]. In addition it was used to predict a decrease in the population abundance variation along with a decrease in population density [2], the relationship between prevalence and abundance given by the epidemiological model developed for macroparasites providing a a measure of aggregation of parasites within their hosts [24] the spatial distribution of plants and animals per unit area [17]. Originally applied in ecology, the use of equation 2 was spread in other sciences such as mathematics in order to show that the variance and the mean of the primes do not exceed a real number sufficiently large obey Taylor's law asymptotically [4]. Finally, in other contexts, a direct scaling analysis was used to estimate the rate of sea level rise at some selected tide gauges around the world [40], in porous media [5,34], and in the framework of fluid mechanics [6,22]. Therefore, the present work aims to validate a theory according to Taylor's Law approach for turbulent flow field and, more precisely, in the context of vortex shedding.

3. Experimental results and discussions

Starting from the signal of voltage fluctuations $\mathbf{v}(t)$ shown in Figure 7 and recorded by the oscilloscope, all values were shifted up, in order to have just strictly positive voltages, according to *Taylor's Law* (equation 2).

Before analyzing the aggregation processes, it was necessary to understand what times scale Δt consider to find a fluctuation scaling. For this purpose, the *autocorrelation coefficient* $\rho(\tau)$, estimable for any stochastic process according to equation 3, was helpful [30]:

$$\rho(\tau) = \frac{C(\tau)}{\sqrt{Var[v(t)]Var[v(t')]}} \tag{3}$$

we recall that the autocovariance $C(\tau)$ is a function corresponding to the covariance, Cov, of the process with itself to pairs of time points, t and t', defined as follows:

$$C(\tau) = C(t, t') = Cov(v(t), v(t')) \tag{4}$$

with time-lag $\tau = t' - t$. Obviously, it must be -1 $\leq \rho(t) \leq 1$. For processes arising in turbulent flows, we expect the autocorrelation $\rho(\tau)$ to diminish as the lag time τ increases. Usually decreases sufficiently rapidly that the integral of equation 3, called integral

Preprints (www.preprints.org) | NOT PEER-REVIEWED | Posted: 14 January 2021 doi:10.20944/preprints202101.0270.v1

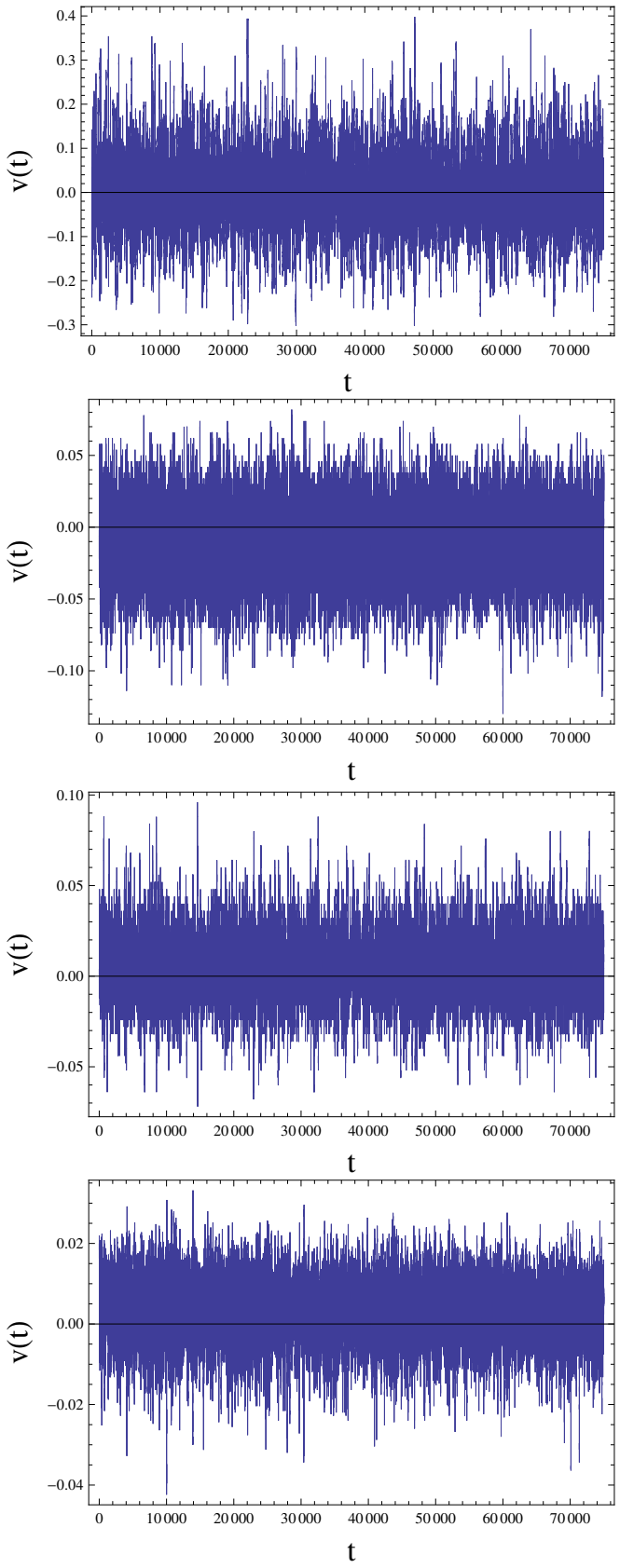

Figure 7. Time history of the fluctuating signals for the following configurations: first (a), second (b), third (c), fourth (d).

Preprints (www.preprints.org) | NOT PEER-REVIEWED | Posted: 14 January 2021 doi:10.20944/preprints202101.0270.v1

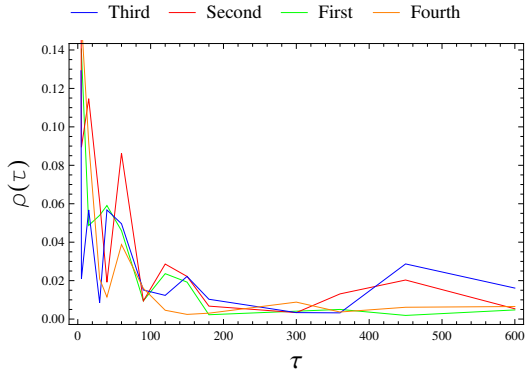

Figure 8. Development of the autocorrelation function over aggregation time for each configuration

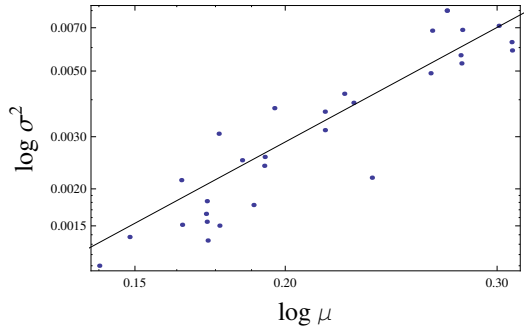

Figure 9. Taylor's law in log-log plane at scale time equal to one minute for the first configuration

timescale of the process, converges:

$$\Gamma = \int_0^{+\infty} \rho(\tau)\, d\tau \tag{5}$$

From a physical point of view, Γ represents the time interval necessary for the process to lose memory of its initial state [39]. The graphs in figure 8 show the trend of autocorrelation function referred to fluctuating signal, which reaches zero value already at a time scale of 3 minutes (for the first, second and fourth configuration) up to a maximum of 5 minutes (for the third configuration), hence voltage fluctuations behave similarly to a turbulent structure. For this reason, our analysis must concern aggregation processes with times scale lower than 3 minutes. Therefore, given a period of fluctuating signal equal to 30 minutes for all the configurations, we consider the following scale times in seconds Δt = 5, 15, 30, 40, 60, 90, 150, 180. For each time scale, the mean and variance were computed and plotted in a bi-logarithmic plane and through a numerical non linear fitting procedure with *Mathematica*©, an interpolating law of equation 2 has been found from the following relationship:

$$\log V = \log a + b \log \mu \tag{6}$$

that represents a linear law in the log-log plane (see figure 9). Once known the parameters of *Taylor's law* a and b (table 1), it was evaluated the correlation coefficient r^2 that represents a measure of fitting degree of the model to data points.

Preprints (www.preprints.org) | NOT PEER-REVIEWED | Posted: 14 January 2021 doi:10.20944/preprints202101.0270.v1

Table 1: Values of scaling exponent of Taylor's law b for each configuration at several aggregation time ranges.

	b			
Δt s	**First** $l = 3.2cm$ $Re = 5944$	**Second** $l = 3.2cm$ $Re = 6835$	**Third** $l = 7.9cm$ $Re = 5944$	**Fourth** $l = 7.9cm$ $Re = 6835$
15	1.773	1.128	1.049	0.875
30	1.951	1.177	1.162	0.957
60	2.197	1.363	1.331	1.055
90	2.262	1.420	1.326	1.031
120	2.330	1.572	1.438	1.071
150	2.440	1,717	1.547	1.244
180	2.496	1.735	1.644	1.148

The values of r^2 relative to each time aggregation range for all the configurations are reported in the table 2.

Table 2: Values of r^2 related to previous fitting laws for each configuration at several aggregation time ranges.

	r^2			
Δt s	**First** $l = 3.2cm$ $Re = 5944$	**Second** $l = 3.2cm$ $Re = 6835$	**Third** $l = 7.9cm$ $Re = 5944$	**Fourth** $l = 7.9cm$ $Re = 6835$
15	0.953	0.964	0.971	0.970
30	0.952	0.967	0.978	0.975
60	0.952	0.964	0.985	0.978
90	0.975	0.964	0.983	0.978
120	0.977	0.966	0.985	0.977
150	0.977	0.973	0.989	0.973
180	0.974	0.971	0.991	0.981

From the values of r^2 in the table 2, it appears that regardless of the configuration and time scale considered the correlation between the experimental data and the fitting Taylor's law is strong, since r^2 is very close to one for all analyses carried out. By table 1, the minimum value of scaling exponent b is 0.875, assumed by the fourth configuration at the time scale equal to 15 seconds, instead the maximum value is 2.496 reached by the first configuration at scale time of 3 minutes. The predominant range is the one between values 1 and 2, typical of the geographical population with relatively moderate degrees of aggregation [21]. The only two configurations characterized by scaling exponents outside this range are the first and the fourth configuration. The scaling law referred to the first configuration presents values of scaling exponent higher than the other configurations. This is reasonable for the highly fluctuating time history of signal (see figure 7a) probably due to the mechanical characteristics of material such as the increase of stiffness inducted by the adapt to fatigue [14]. Instead, the fourth configuration is characterized by lowest values of scaling exponent since the fluctuating signal is almost homogeneous (see figure 7d). From a general point of view, the scale exponent b increases with the aggregation time Δt, no matter the configuration. According to the least squares method, both linear (figure 10a) and logarithmic law (figure 10b) have been found in order to maximize the correlation coefficient r^2, consequently it has pointed out the logarithmic law is the best fitting line given that the scale exponent grows slightly with the aggregation time.

With reference to the earlier cases of application of Taylor's law, a logarithmic trend of scaling exponent on aggregation time has also been found by [15] investigating the endogenous and exogenous dynamics of 1354 stocks traded in the Chinese stock market. In

Preprints (www.preprints.org) | NOT PEER-REVIEWED | Posted: 14 January 2021 doi:10.20944/preprints202101.0270.v1

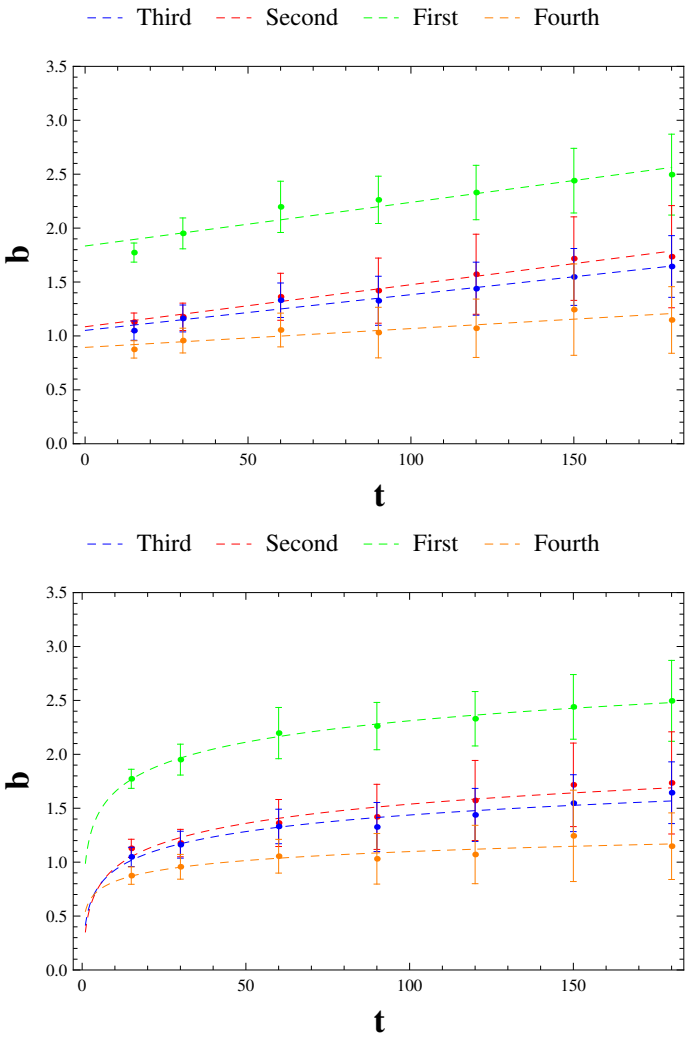

Figure 10. Laws of variation of scaling exponent over the aggregation time: linear law (a) and logarithmic law (b).

Preprints (www.preprints.org) | NOT PEER-REVIEWED | Posted: 14 January 2021 doi:10.20944/preprints202101.0270.v1

addition, analyzing the time series of trading volume of 22 liquid stocks traded on Shenzen Stock Exchange in 2003, Mu et al [25] reached the same outcome. Based on the previous results, we can state a general variation law of the scaling exponent over scale time:

$$b(\Delta t) = b_0 + k \log \Delta t \tag{7}$$

The values of b_0 and k related to the configurations are summarized in the table 3, by which we can deduce that b_0 varies strongly with the configuration considered hence probably it depends on the flag length and height of the open channel, while k belongs to the narrow range between 0.12 and 0.28.

Table 3: Values of b_0 and k for the logarithmic laws.

	First	Second	Third	Fourth
b_0	0.989	0.353	0.416	0.544
k	0.287	0.257	0.222	0.120

At this point, it is important to understand how the fluctuations $\mathbf{v}(t)$ are distributed. If we plot in a plane (figure 11) whose horizontal axis represents the values of voltage $\mathbf{v}(t)$ and the vertical axis the frequency distribution f_V with a width bin equal to 0.001 volts, we obtain the histogram of frequency from which we can make some considerations for each configuration analyzed.

For example, the first configuration (see figure 11a), given its shape, is characterized by a considerable degree of uncertainty. This means that the distribution has a high standard deviation according to results listed in the table 1. In the second and third configuration we notice the presence of skewness, with a tail on the right side in the second (see figure 11b) and a tail on the left side in the third (see figure 11c). The fourth configuration (see figure 11d), has the lowest standard deviation according to highly homogeneous shape of fluctuating signal. Then, a comparison between the histogram of frequency and some theoretical probability density function has been carried out. Anyway, by means the Method of Moments, it appears that the probability density function that more likehoods to the real distributions of the voltage fluctuations $\mathbf{v}(t)$ is the Gaussian one. This result is in agreement with the experimental evidence and numerical simulations as well-known in literature [7,30,39,41,42]. Therefore, based on this encouraging preliminary survey, several geometric analysis in the channel flume will be carried out in order to validate this sensor in other ranges of Strouhal and Reynolds number. This validation will be accompanied by relationship between voltage fluctuations and chaotic components of the fully developed turbulent speed ($\mathbf{v}(t) \sim u'(t)$) once known the average flow field around the cylinder, with and without the flag.

4. Conclusions

In the presented work, a scaling analysis of measure fluctuations on a flapping flag thin-films based device has been carried out in a channel flume site in EUMER Lab at University of Salento for a specific range of the order of $Re = 10^4$. In the preliminary stage, based on the dimensional analysis, we have introduced Strouhal number, as known in the literature, regardless the flag length, at a flow field for which experimental data are in the plateau zone of $St = 0.21$. It has been estimated, for each analyzed configuration, the autocorrelation coefficient that shows an ergodic behavior of the signal and the scale times within which turbulent structure is coherent. Consequently, it has been possible to demonstrate that fluctuations of the flapping flag respond to the Taylor's law applied in several scientific and technical contexts, with the scaling exponents convergent in a particular range between 0.8 and 2.5. This has allowed us to determine an invariant scale between the voltage fluctuations and chaotic components of the fully developed turbulent speed for the flow field considered. Finally, by comparison between the frequency

Preprints (www.preprints.org) | NOT PEER-REVIEWED | Posted: 14 January 2021 doi:10.20944/preprints202101.0270.v1

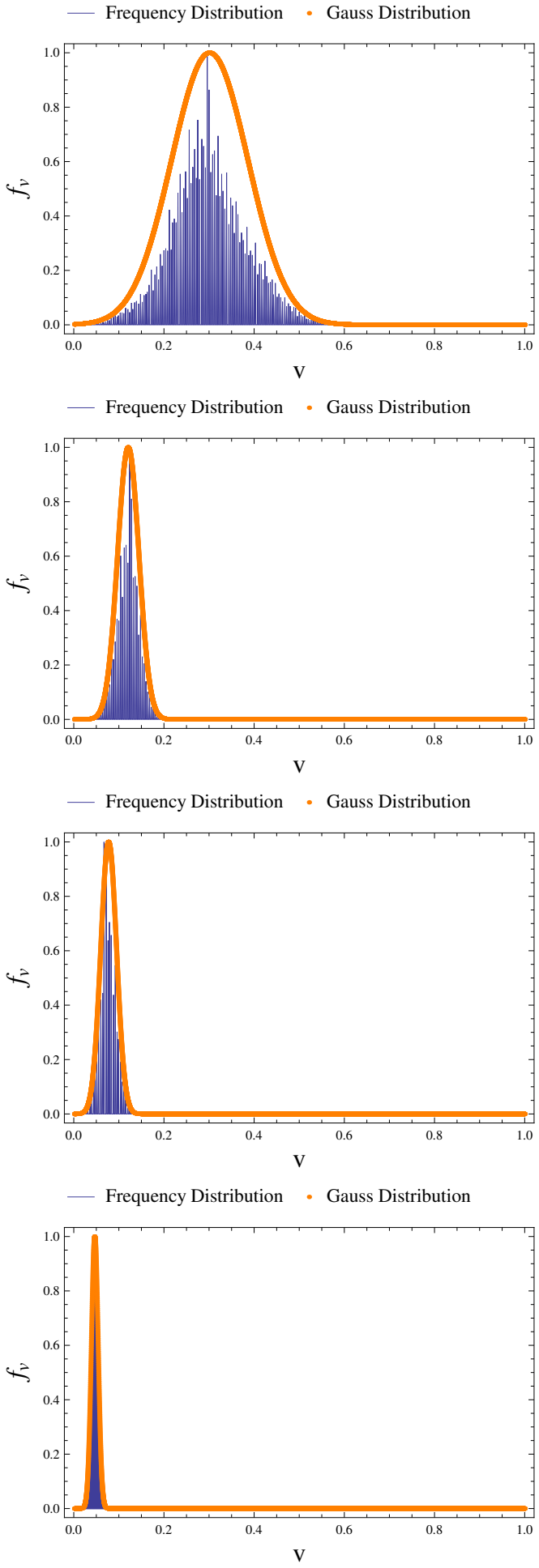

Figure 11. Comparison between the observed frequency distribution and the Gaussian probability density function

distribution of voltages and some theoretical probability density functions, it has been found that the maximum similarity is reached with the Gaussian distribution. With these considerations, we can say that the thin-films based device is able to provide several information on the flow field. Further investigations are being planned to validate other orders of Reynolds number in order to find out if the scaling behavior of Taylor's law could be applicable as well.

Funding: This research received no external funding

Acknowledgments: The thin-films based device was provided by Piezoskin Startup of the Italian Institute of Technology (IIT) based in Lecce (Italy). The performance of device were tested both in the European Maritime and Environmental Research (EUMER) Laboratory located inside the University of Salento and in the Italian Institute of Technology (IIT).

Conflicts of Interest: The authors declare no conflict of interest.

References

1. Algieri, L.; Todaro, M. T.; Guido, F.; Mastronardi, V.; Desmaële, D.; Qualtieri, A.; Giannini, C.; Sibillano, T; and De Vittorio, M. Flexible Piezoelectric Energy-Harvesting Exploiting Biocompatible AlN Thin Films Grown onto Spin-Coated Polyimide Layers *ACS Applied Energy Materials* **1(10)**, 5203–5210.
2. Anile, S. and Devillard, S. Spatial variance-mass allometry of population density in felids from camera-trapping studies worldwide *Scientific Reports* **10**, 14814.
3. Bearman, P. Investigation of the flow behind a two-dimensional model with a blunt trailing edge and fitted with splitter plates *Journal of Fluid Mechanicss* **21(2)**, 241–255.
4. Cohen, J. E. Statistics of primes (and probably twin primes) satisfy Taylor's Law from ecology, *The American Statistician*, **70(4)**, 399–404.
5. De Bartolo, S.; Fallico, C.; Severino, G. A fractal analysis of the water retention curve, Hydrological Processes, *Hydrologic Processes*, **32(10)**, 1401–1405.
6. De Silva, C. M.; Marusic, I.; Woodcock, J. D.; Meneveau, C Scaling of second-and higher-order structure functions in turbulent boundary layers, *Journal of Fluid Mechanics*, **769**, 654–686.
7. Durst, F.; Launder, B. E.; Lumley, J. L.; Schmidt, F. W. and Whitelaw, J. H. Turbulent Shear Flows 5, *Cornell University, Ithaca, New York, USA.*
8. Eisler, Z.; Bartos, I. and Kertesz J. Fluctuation scaling in complex systems: Taylor's Law and beyond, *Advances in Physics*, **57(1)**, 89–142.
9. Eloy, C. Optimal Strouhal number for swimming animals, *Journal of Fluids and Structures*, **30**, 205–218.
10. Fronczak, A. and Fronczak, P. Origins of Taylor's power law for fluctuation scaling in complex systems, *Physical Review E*, **81**.
11. Giometto, A.; Formentin, M.; Rinaldo, A.; Cohen, J. E.; Maritan, A. Sample and population exponents of generalized Taylor's law *Proceedings of the National Academy of Sciences of the United States of America*, **112(25)**.
12. Gonçalves, H. C. and Vieira, E. D. R. Strouhal Number Determination for Several Regular Polygon Cylinders for Reynolds Number up to 600, *XV Congresso Brasileiro de Engenharia Mecânica*, **10 pp**.
13. Griffin, O. M. A universal Strouhal number for the 'locking-on' of vortex shedding to the vibrations of bluff cylinders, *Journal of Fluid Mechanics*, **85(3)**, 591–606.
14. Jendzelovsky, N. and Antal, R. Fluid-Structure Interaction Analysis and the Detection of Wind Induced Vibration of Triangular Lamella, *IOP Conf. Ser.: Mater. Sci. Eng*, **471**, 052009.
15. Jiang, Z.-Q.; Guo, L. and Zhou, W.-X. Endogenous and exogenous dynamics in the fluctuation of capital fluxe, *The European Physical Journal B*, **57**, 347–355.
16. Katopodes, D.N. Free surface flow: environmental fluid mechanics, *Elsevier Science and Technology*.
17. Kendal, W. S. A probabilistic model for the variance to mean power law in ecology, *Ecological Modelling*, **80**, 293–297.
18. Kendal, W.S. and Jorgensen, B. Taylor's power law and fluctuation scaling explained by a central-limit-like convergence, *Physical Review E*, **83**.

19. Madaro, F., Mehdipour, I., Caricato, A., Guido, F., Rizzi, F., Carlucci, A. P., De Vittorio, M. Available Energy in Cars' Exhaust System for IoT Remote Exhaust Gas Sensor and Piezoelectric Harvesting, *Energies*, **13(6)**, 4169.
20. Manela, A. and Howe M. S. The forced motion of a flag, *J. Fluid Mech.*, **635**, pp. 439–454.
21. Maurer, B. A. and Taper, M. L. Connecting geographical distributions with population processes, *Ecology Letters*, **5**, 223–231.
22. Meneveau, C., Sreenivasan, K. R. The multifractal nature of turbulent energy dissipation, *Journal of Fluid Mechanics*, **224**, 429–484.
23. Michelin, S.; LLewellyn Smith, S.G. and Glover B. J. Vortex shedding model of a flapping flag, *Journal of Fluid Mechanics.*, **617**, pp. 1–10.
24. Morand, S. and Krasnov, B. (2008) Why apply ecological laws to epidemiology?, *Trends in Parasitology*, **24(7)**, 304–309.
25. Mu, G.-H.; Zhou, W.-X.; Chen, W. and Kertész, J.Long-term correlations and multifractality in trading volumes for Chinese stocks, *Physics Procedia*, **3 (5)**, 1631–1640.
26. Nieradka, K.; Kopiec, D.; Małozięć, G.; Kowalska, Z.; Grabiec, P.; Janus, P.; Sierakowski, A.; Domański, K. and Gotszalk, T. Fabrication and characterization of electromagnetically actuated microcantilevers for biochemical sensing, parallel AFM and nanomanipulation, *Microelectronic Engineering*, **98**, 676–679.
27. Okajima, A. Strouhal numbers of rectangular cylinders, *Journal of Fluid Mechanics*, **123**, 379–398.
28. Petroni, S.; Rizzi, F.; Guido, F.; Cannavale, A.; Donateo,T.; Ingrosso, F.; Mastronardi, V.; Cingolani, R. and De Vittorio, M.Flexible AlN flags for efficient wind energy harvesting at ultralow cut-in wind speed, *RSC Advances*, **5**, 14047–14052.
29. Pobering, S.; Ebermeyer, S. and Schwesinger, N. Generation of electrical energy using short piezoelectric cantilevers in flowing media, *Smart Structures and Materials + Nondestructive Evaluation and Health Monitoring*.
30. Pope, S.B. Turbulent flows *Cambridge University Press*.
31. Rodriguez, I., Lehmkul, O., Chiva, J., Borrell, R. and Oliva, A. On the flow past a circular cylinder from critical to super-critical Reynolds numbers: Wake topology and vortex shedding *International Journal of Heat and Fluid Flow*, **55**, 91–103.
32. Roshko, A. On the development of turbulent wakes from vortex streets, *Dissertation (Ph.D.), California Institute of Technology*.
33. Roshko, A. Experiments on the flow past a circular cylinder at very high Reynolds number, *Journal of Fluid Mechanics*, **10(3)**,345–356.
34. Severino, G. and De Bartolo, S. A scale invariant property of the water retention curve in weakly heterogeneous vadose zone, *Hydrologic Processes*, **33(7)**, 1032–1039.
35. Shi, L.; Yu, Z.; and Jaworski, A. J. Investigation into the Strouhal numbers associated with vortex shedding from parallel-plate thermoacoustic stacks in oscillatory flow conditions, *European Journal of Mechanics - B/Fluids*, **30**, 206–217.
36. Strouhal, V. Ueber eine besondere Art der Tonerregung, *Annalen der Physik und Chemie*, **241(10)**, 216–251.
37. Taylor, L. Aggregation, Variance and the Mean, *Nature*, **189**, 732–735.
38. Taylor, G.K.; Nudds, R.L.; Thomas, A.L.R. Flying and swimming animals cruise at a Strouhal number tuned for high power efficiency, *Nature*, **2913**.
39. Tennekes, H. and Lumley, J.L. A first course in turbulence, *MIT Press*.
40. Tomasicchio, G. R.; Lusito, L.; D'Alessandro, F.; Frega, F.; Francone, A. and De Bartolo, S. (2018) A direct scaling analysis for the sea level rise, *Stochastic Environmental Research and Risk Assessment*, **32**, 3397-–3408.
41. Townsend, A. A. The Structure of Turbulent Shear Flow, 2nd edition. *Cambridge University Press*.
42. Yamamoto, K. and Kambe,T. Gaussian and near-exponential probability distributions of turbulence obtained from a numerical simulation, *Fluid Dynamic Research*, **8**, 65–72.

Sample Availability: Samples of the compounds ..... are available from the authors.

 doi:10.20944/preprints202101.0270.v1